

# High-Gravity-Assisted Synthesis of Surfactant-Free Transparent Dispersions of Monodispersed MgAl-LDH Nanoparticles

Bo Chen, Qian Sun, Dan Wang, Xiao-Fei Zeng, Jie-Xin Wang,\* and Jian-Feng Chen

Cite This: *Ind. Eng. Chem. Res.* 2020, 59, 2960–2967

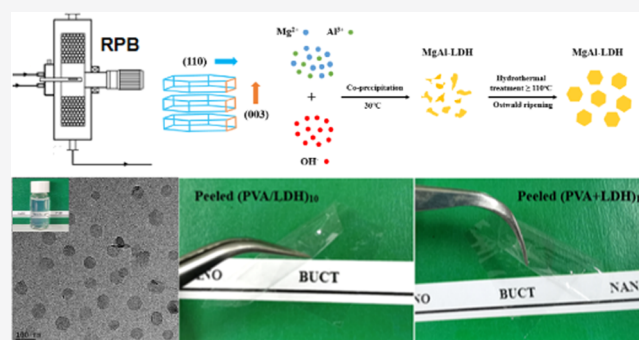
Read Online

ACCESS |

Metrics & More

Article Recommendations

**ABSTRACT:** As a family of important inorganic layered materials, layered double hydroxides (LDHs) have attracted considerable attention owing to their potential applications in wide areas. Generally, the size, shape, uniformity, and dispersity of LDHs have great effects on their application properties. Herein, we report an efficient approach to prepare surfactant-free transparent dispersions of monodispersed  $\text{CO}_3^{2-}$ -intercalated MgAl-LDH nanoparticles using a high-gravity-assisted intensified coprecipitation method in a rotating packed-bed (RPB) reactor, followed by hydrothermal treatment. After a rapid coprecipitation in the RPB reactor, monodispersed MgAl-LDH nanoparticles with an average particle size of about 31 nm can be obtained. As compared to that in a stirred tank reactor (STR), the product from the RPB has a much smaller particle size, narrower size distribution, and higher optical transparency. More importantly, the reaction time can be significantly reduced from 20 min to 20 s, realizing an efficient continuous preparation. Subsequent hydrothermal treatment will facilitate the particles to change from irregular shapes to hexagonal nanoflakes. Simultaneously, the average particle size of MgAl-LDH nanoparticles rises to 65–72 nm on increasing the hydrothermal temperature from 90 to 130 °C. Furthermore, highly transparent and flexible nanocomposite films consisting of poly(vinyl alcohol) (PVA) and MgAl-LDH nanoparticles are readily fabricated with the spin-coating method and the layer-by-layer technique. It could be envisioned that such LDH dispersions may have a wide range of potential applications in the fields of optical devices, catalysis, gas separation, sensing, and antflaming materials.



## 1. INTRODUCTION

Layered double hydroxides (LDHs) are a class of anionic clay materials composed of positively charged hydrotalcite-like layers and interlayered galleries containing counterions and solvation molecules. The general formula of LDHs can be described as  $[\text{M(II)}_{1-x}\text{M(III)}_x(\text{OH})_2][\text{A}^{n-}]_{x/n} \cdot z\text{H}_2\text{O}$ , where M(II) and M(III) are usually divalent and trivalent metal cations, respectively, and  $\text{A}^{n-}$  is the intercalated anion. Most commonly, M(II) can be chosen from  $\text{Mg}^{2+}$ ,  $\text{Zn}^{2+}$ ,  $\text{Cu}^{2+}$ ,  $\text{Co}^{2+}$ , and  $\text{Ni}^{2+}$ , and M(III) can be chosen from  $\text{Al}^{3+}$ ,  $\text{Fe}^{3+}$ ,  $\text{Mn}^{3+}$ ,  $\text{Cr}^{3+}$ , etc.  $\text{A}^{n-}$  plays a role in neutralizing the positive charges provided by bimetallic layers, and it is often selected from  $\text{Cl}^-$ ,  $\text{NO}_3^-$ ,  $\text{CO}_3^{2-}$ ,  $\text{SO}_4^{2-}$ , or  $\text{PO}_4^{3-}$ .<sup>1–3</sup> In recent decades, LDHs have been extensively studied for their applications in both scientific research and industries, due to their excellent physical and chemical properties in ion exchange, structural controllability, memory effect, fire resistance, and functions of exfoliation and reconstruction. For example, they can be applied in the preparation of ion-exchange hosts, acid gas absorbents, catalysts, and fire retardants. In addition, they are also ideal raw materials or precursors for preparing catalyst carriers, self-assembled materials, optical devices, and biomaterials.<sup>4–7</sup>

Among numerous kinds of LDHs, MgAl-LDHs are the earliest and deepest researched products. So far, there have been a number of methods to prepare MgAl-LDHs, such as coprecipitation, hydrothermal treatment, ion exchange, hydrolysis of alkoxides, and reverse microemulsion.<sup>8–12</sup> Among all of these approaches, coprecipitation of metallic salts is the most fundamental and commonly used one. However, by using this method, MgAl-LDH particles are usually obtained with irregular shapes and broad size distributions because of the variation of the solution supersaturation degree during a reaction in a traditional stirred tank reactor (STR). Particles precipitated at the beginning undergo a much longer growth period than those precipitated at the end and thus have much larger particle sizes. In addition, particle aggregation happens to most current products due to the attraction between

Received: November 14, 2019

Revised: January 21, 2020

Accepted: January 22, 2020

Published: January 22, 2020

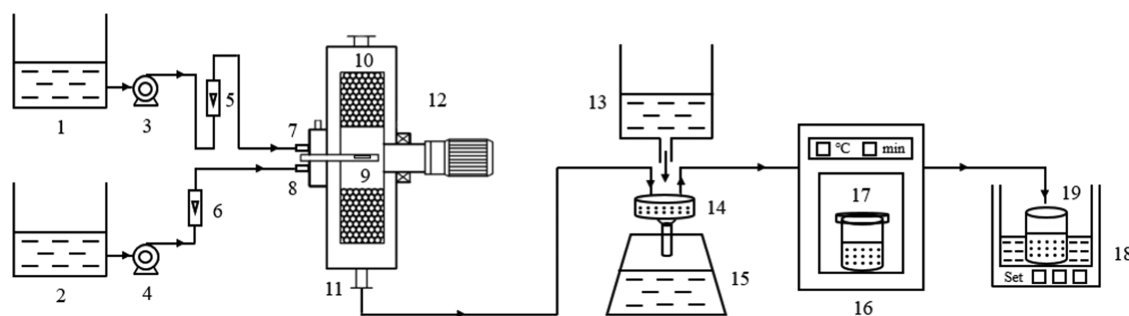


**Figure 1.** Illustration of the experimental setup for an RPB experiment: (1)  $\text{Mg}^{2+}/\text{Al}^{3+}$  salt solution tank, (2)  $\text{NH}_3\cdot\text{H}_2\text{O}$  solution tank, (3–4) pump, (5–6) flowmeter, (7–8) inlet, (9) slotted pipe, (10) stainless wire mesh packing, (11) outlet, (12) RPB reactor, (13) ultrapure water tank, (14) funnel, (15) filter flask, (16) digital oven, (17) autoclave, (18) sonicator, and (19) dispersion of MgAl-LDH nanoparticles.

different particles, which will seriously deteriorate the mechanical properties and application performance of products.<sup>13,14</sup> Thus, it is still a challenge for us to realize the efficient preparation of high-quality MgAl-LDHs with small sizes, regular shapes, and excellent dispersibility.

Monodispersed nanoparticles, which exhibit a lot of size- and shape-dependent phenomena, have been studied in depth due to their excellent dispersibility, specific morphologies, and functions as building blocks in synthesizing advanced materials. In the past decade, many monodispersed nanoparticles have been achieved, including noble metals, metal oxides, and some other metallic compounds.<sup>15–17</sup> However, monodispersed nanoparticles of metal hydroxides have been rarely reported, especially for LDHs. Duan and co-workers realized the preparation of MgAl- $\text{CO}_3$  LDH nanoparticles with the size of 60–80 nm using a colloid mill followed by a separate aging process. However, most of these single particles were attached to each other to form chains or were aggregated in the microscale.<sup>18</sup> Pang et al. synthesized naked  $\text{Mg}_2\text{Al}(\text{NO}_3)_2$  LDH nanosheets by a coprecipitation method using a T-type microchannel reactor.<sup>19</sup> The nanosheets were obtained with thickness of 0.68–1.13 nm and lateral size of 20–30 nm. However, these nanosheets can be steadily dispersed into aqueous solutions for only 16 h at room temperature. In recent years, more advanced techniques have been developed to synthesize LDH nanoparticles or nanomaterials, but the disadvantages of most approaches are obvious and very difficult to be avoided.<sup>20–22</sup> Therefore, it is worth developing a facile and efficient method to synthesize monodispersed LDH nanoparticles.

Rotating packed bed (RPB) is a kind of novel reactor that can generate an environment with highly intensified micro-mixing and mass transfer<sup>23,24</sup> and has been successfully employed to synthesize different nanomaterials with uniform sizes and regular morphologies, such as Ag, ZnO,  $\text{CaCO}_3$ , and  $\text{Mg}(\text{OH})_2$ .<sup>25–28</sup> Therefore, RPB is a very promising platform for preparing monodispersed LDH nanoparticles. Recently, many researchers have attempted to synthesize LDH nanoparticles in a high-gravity environment, but most of them did not achieve particles in the nanoscale ( $\leq 100$  nm). For example, an impinging stream–rotating packed-bed (IS-RPB) reactor was used with a coprecipitation method to prepare CoMn-LDH by Zhang et al.<sup>29</sup> According to their results of scanning electron microscope (SEM) and dynamic light-scattering, the particles were obtained with an average particle size of 187.9 nm. Similarly, Xu and co-workers prepared MgAl-LDHs using a high-gravity-reactive precipitation method, but the particles were obtained with an average particle size of 160

nm and a broad size distribution ranges from 46 to 478 nm.<sup>30</sup> Compared with previous studies by the RPB reactor or some other continuous flow reactors,<sup>31–33</sup> our study reveals an efficient approach for synthesizing surfactant-free monodispersed MgAl- $\text{CO}_3$  LDH nanoparticles using a high-gravity-assisted coprecipitation method in an RPB reactor combined with hydrothermal treatment. The as-prepared nanoparticles were obtained with average particle size range from ca. 30 to 70 nm and can be easily dispersed into water to form stable ( $\geq 6$  months) and transparent aqueous suspensions. A traditional STR experiment was also carried out for comparison. Furthermore, nanocomposite films containing poly(vinyl alcohol) (PVA) and MgAl-LDH nanoparticles were also successfully fabricated with excellent optical transparency and flexibility.

## 2. EXPERIMENTAL SECTION

**2.1. Chemicals and Reagents.** Aluminum nitrate nonahydrate ( $\text{Al}(\text{NO}_3)_3\cdot 9\text{H}_2\text{O}$ ,  $\geq 99\%$ ), magnesium nitrate hexahydrate ( $\text{Mg}(\text{NO}_3)_2\cdot 6\text{H}_2\text{O}$ ,  $\geq 99\%$ ), and ammonium hydroxide ( $\text{NH}_3\cdot\text{H}_2\text{O}$ , 25–28%) were purchased from Tianjin Fuchen Chemical Reagents Factory (China). Sulfuric acid ( $\text{H}_2\text{SO}_4$ ,  $\geq 98\%$ ), hydrogen peroxide ( $\text{H}_2\text{O}_2$ ,  $\geq 30\%$ ), and poly(vinyl alcohol) (PVA, #1788, molar mass: 44.05) were obtained from Beijing Chemical Reagent Co., Ltd. (China). All chemicals and reagents used in these experiments are analytical-grade pure and were used without further purification. Ultrapure water ( $18.2\text{ M}\Omega\cdot\text{cm}$ ) was produced by a Laboratory Water Purification System (Smart-S30) from Shanghai Hitech Instruments Co., Ltd. (China).

**2.2. Equipment.** The rotating packed bed (RPB) used in this work consists of a rotor and porous stainless wire mesh packing, and it is designed with two reactant inlets and one product outlet. The rotor is twined with the packing, whose porosity and specific surface area are 0.9 and  $850\text{ m}^2/\text{m}^3$ , respectively. The inside and outside diameters of the rotor are 46 and 92 mm, respectively, and the axial length of the rotor is 44 mm. More details about the RPB have been reported in our previous publications.<sup>34,35</sup> Figure 1 shows the experimental setup of the entire process, including homogeneous coprecipitation in the RPB reactor and hydrothermal treatment.

**2.3. Preparation of Transparent Dispersions of Monodispersed MgAl-LDH Nanoparticles.** In a typical synthesis process, 5.769 g of  $\text{Mg}(\text{NO}_3)_2\cdot 6\text{H}_2\text{O}$  and 2.813 g of  $\text{Al}(\text{NO}_3)_3\cdot 9\text{H}_2\text{O}$  were dissolved in 100 mL of ultrapure water to form solution A, and 20 mL of  $\text{NH}_3\cdot\text{H}_2\text{O}$  (25–28%) was diluted to 100 mL to form solution B. Solution A and solution

B were stored separately in two beakers and heated to 30 °C by a digital water bath. At the beginning of coprecipitation, two liquid streams containing metal salts and  $\text{NH}_3 \cdot \text{H}_2\text{O}$  were pumped into the interior of RPB, sequentially, and then sprayed onto the inside edge of the rotor. The flow rates were controlled at 300 mL/min by flowmeters, and the liquid streams were uniformly and rapidly distributed by slotted pipes. Afterward, the two liquid streams were vigorously mixed and reacted with each other in the packing zone to generate a white suspension of MgAl-LDH nanoparticles. The residence time of the generated suspension was ca. 1 s, much shorter than that conducted by an STR reactor or some other continuous flow reactors. Subsequently, the resulting suspension was collected from the outlet and filtered and rinsed with ultrapure water several times by a Buchner funnel. The funnel was covered with a qualitative filter paper and two polyamide filter membranes in sequence, whose pore sizes were 20 and 0.1  $\mu\text{m}$ , respectively. After that, a clean filter cake and a completely transparent filtrate were separately obtained in the funnel and filter flask. Then, the filter cake was redispersed into ultrapure water to form a transparent dispersion of monodispersed MgAl-LDH nanoparticles.

Furthermore, hydrothermal treatment was immediately carried out to investigate the effect of aging on particle size and morphology. Specifically, the above-obtained transparent dispersion was placed in a sealed Teflon-lined stainless steel autoclave and heated to a certain temperature for 12 h. After that, the autoclave was cooled down to room temperature, and the resulting dispersion was recovered.

A traditional STR experiment was also conducted for comparison with the RPB-prepared products, and all reaction conditions including solution concentrations, temperatures, and heating time set for an STR experiment were the same as set for an RPB experiment. However, solution B was added dropwise to solution A in an STR experiment, which took up to 20 min to finish a circle, much longer than the 20 s needed by an RPB. After that, the rest of the steps were performed under the same conditions as in an RPB experiment. According to the reaction time and powder mass obtained by drying the MgAl-LDH dispersions, we can calculate that the productivities of the RPB reactor and the STR reactor were 315 and 5.25 g/h, respectively. Obviously, the RPB achieved a yield that was 60 times that of the STR, indicating its high efficiency in producing MgAl-LDH nanoparticles.

**2.4. Fabrication of Transparent Nanocomposite Films.** Nanocomposite films of  $(\text{PVA/LDH})_n$  and  $(\text{PVA} + \text{LDH})_n$  ( $n = 1-10$ ) were fabricated by using the spin-coating method and the layer-by-layer technique. Quartz glass was chosen as the substrate and precleaned with Piranha solution (70%  $\text{H}_2\text{SO}_4$  + 30%  $\text{H}_2\text{O}_2$ ) before experiments. First, the PVA solution (5 wt %) was prepared by dissolving a certain amount of PVA powders into ultrapure water with heating and stirring at 98 °C. Then, the PVA solution was cooled down to room temperature and spin-coated onto the surface of the pretreated quartz glass substrate. The film was dried at room temperature and subsequently coated with the as-prepared transparent dispersion of monodispersed MgAl-LDH nanoparticles. The PVA/LDH film was obtained after drying again, and the  $(\text{PVA/LDH})_n$  films can be prepared by repeating the above operations “ $n$ ” times.

Similarly, the  $(\text{PVA} + \text{LDH})_n$  films can also be fabricated by the above procedures. The only difference is that the PVA solution was intensively mixed with the transparent dispersion

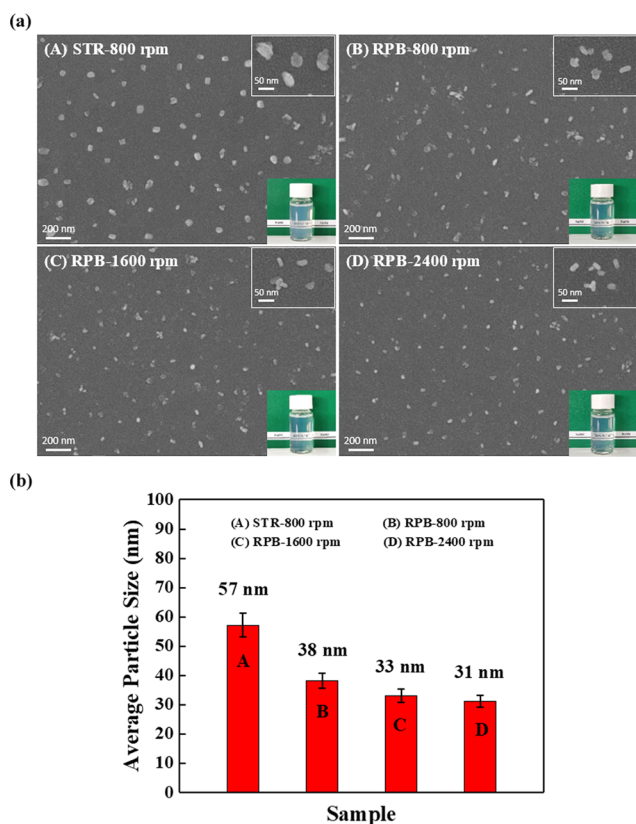
of monodispersed MgAl-LDH nanoparticles before coating for the purpose of testing the compatibility between PVA and MgAl-LDH nanoparticles. As a result, a two-component film was generated after the mixed solution was coated onto the quartz glass and dried later, and the  $(\text{PVA} + \text{LDH})_n$  films can be easily obtained by repeating the coating and drying procedures “ $n$ ” times alternatively.

**2.5. Characterization.** The particle size and morphology of MgAl-LDH nanoparticles were observed using a scanning electron microscope (SEM) (JSM-6701, JEOL, Japan) and a transmission electron microscope (TEM) (JEM-2010F, JEOL, Japan). The X-ray diffraction (XRD) pattern of MgAl-LDH nanopowders was recorded using an X-ray diffractometer (XRD-6000, Shimadzu, Japan) in the scanning range of 5–70°. The Fourier transform infrared (FT-IR) spectrum of MgAl-LDH nanoparticles was detected by a Nicolet 6700 spectrometer (Nicolet Instrument Co.) in the wavenumber range of 4000–400  $\text{cm}^{-1}$ . The light transmittance of the as-prepared dispersions was assessed through a UV-vis spectrometer (UV-2501, Shimadzu, Japan) within the scope of 200–800 nm. The  $\zeta$ -potential of MgAl-LDH nanoparticles dispersed in the aqueous solution was detected through a  $\zeta$ -potential analyzer (Nano ZS-90, Malvern Instrument Ltd., U.K.) at 25 °C. The thermal behavior of MgAl-LDH nanoparticles was investigated via a thermal gravimetric analysis (TGA) system (TGA/DSC1 SF 1100, Mettler Toledo, Switzerland) at a heating rate of 10 °C·min<sup>−1</sup> in air.

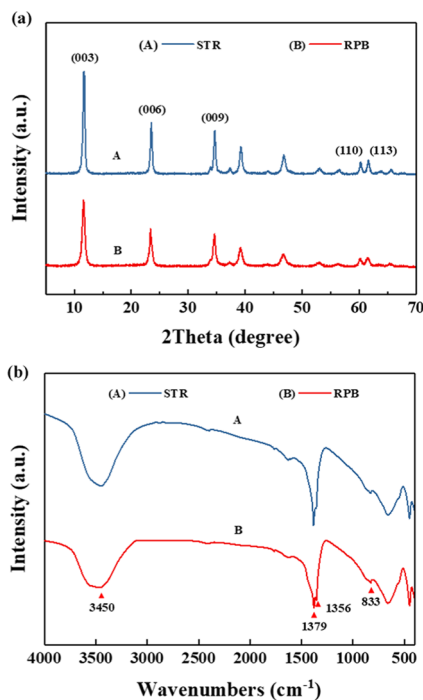
### 3. RESULTS AND DISCUSSION

Figure 2a shows the SEM images of MgAl-LDH nanoparticles prepared by an STR or RPB, and their corresponding digital photographs of dispersions are shown in the inset. The stirring speed was set to 800 rpm for an STR experiment. In comparison, 800, 1600, and 2400 rpm were set, respectively, for the three RPB experiments. The average particle size of each sample was calculated by statistics, and the result is shown in Figure 2b; over 50 particles were randomly collected for each sample. Clearly, monodispersed MgAl-LDH nanoparticles with irregular shapes were prepared for all samples under these experimental conditions. However, the reaction time was reduced from 20 min by an STR to 20 s by an RPB, and the RPB-prepared nanoparticles have much smaller sizes and narrower size distributions. According to the statistics, 57, 38, 33, and 31 nm are counted as the results of the average particle size for those four samples. As mentioned in our previous publications, the liquid streams passing through the packing zone can be fast divided into countless tiny droplets or thin films, thereby resulting in a high specific surface area and intensifying the micromixing and mass transfer of reactants.<sup>36,37</sup> Therefore, the rapid nucleation and much shorter growth period of particles in an RPB will result in smaller average particle sizes and more uniform size distributions than those in an STR. In addition, the rotating speed of RPB represents the intensity of micromixing and mass transfer; thus, the average particle size gradually decreases with the increase of rotating speed.

Figure 3 displays the representative XRD patterns and FT-IR spectra of two samples prepared in an STR and RPB, respectively, with a stirring/rotating speed of 800 rpm. It can be obviously seen that both samples are obtained with a typical parallel layered structure, which is evidenced by the appearance of XRD peaks located at  $2\theta = 11.62^\circ$ ,  $23.38^\circ$ , and  $34.62^\circ$ . According to JCPDS 51-1528, the three above-mentioned



**Figure 2.** (a) SEM images and (b) the corresponding average particle sizes of MgAl-LDH nanoparticles prepared by (A) STR-800 rpm, (B) RPB-800 rpm, (C) RPB-1600 rpm, and (D) RPB-2400 rpm.



**Figure 3.** (a) XRD patterns and (b) FT-IR spectra of MgAl-LDH nanoparticles prepared using an STR and RPB, respectively, with a stirring/rotating speed of 800 rpm.

peaks correspond to the characteristic reflections of hydro-talcite on crystal planes of (003), (006), and (009). In

addition,  $d(003) = 0.76$  nm is calculated by Bragg's law, which indicates that the as-prepared MgAl-LDH nanoparticles are  $\text{CO}_3^{2-}$  intercalated. This demonstrates that the MgAl- $\text{CO}_3$  LDH nanoparticles can be successfully prepared by this homogeneous coprecipitation method. Moreover, the RPB-prepared sample exhibits a slightly broader width of peaks than that of the STR-prepared one, which means that the RPB-prepared sample has a smaller average particle size. The Debye–Scherrer equation is applied to calculate the crystal size in terms of the (110) plane. As a result, 52.8 and 37.7 nm are acquired for sample A and sample B, respectively. These are approximately consistent with the SEM results. The FT-IR absorption peaks at 1379, 1356, and 833  $\text{cm}^{-1}$  are ascribed to the antisymmetric stretching vibration and out-of-plane bending vibration of  $\text{CO}_3^{2-}$ , which is consistent with the XRD result. The other peaks occur at 3450 and 750–480  $\text{cm}^{-1}$  are assigned to the stretching vibration of O–H in water and the stretching and bending vibrations of metal–O groups. All of the above pieces of evidence suggest that the  $\text{CO}_3^{2-}$ -intercalated MgAl-LDHs were successfully prepared by both an STR and RPB. In addition, no peaks arising from impurities are detected in XRD and FT-IR curves, indicating that the products have high levels of purity.

Figure 4 exhibits the as-prepared four sample dispersions containing MgAl-LDH nanoparticles synthesized by an STR or

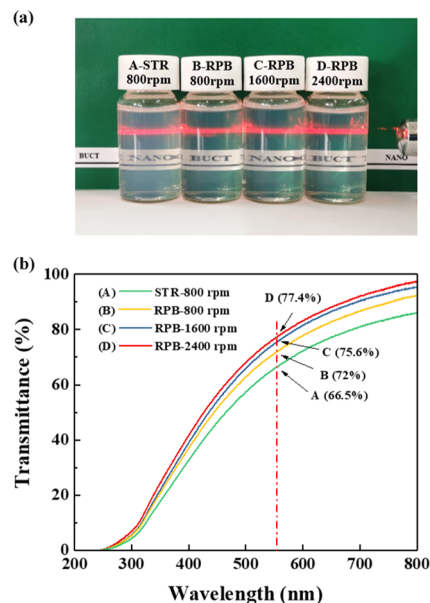


**Figure 4.** (a) Photographs of dispersions (1 wt %) of the MgAl-LDH nanoparticles prepared using an STR or RPB, and (b) their corresponding UV-vis test curves on light transmittance.

RPB and their corresponding UV-vis test results on light transmittance. All dispersions were prepared with the same concentration of 1 wt %. It is remarkable that the samples prepared by an RPB have better visual transparency than those prepared by an STR. Furthermore, the Tyndall effect can be observed for every sample, which illustrates an excellent dispersibility of the as-prepared MgAl-LDH nanoparticles in the aqueous solution. According to the light transmittance curves, all samples are detected to have high levels of light transmission in the visible-light region. It is well known that human eyes are the most sensitive to green light at about 555 nm. Accordingly, values of 77.4, 75.6, 72, and 66.5% are

detected for those four samples at the above-mentioned wavelength. Clearly, the worst performance was from the STR-prepared sample, which should be responsible for the lowest optical transparency of dispersions. As depicted by Rayleigh scattering, the intensity of scattered light increases with the rise of particle size, thereby leading to the decline of visible-light transmission. In addition, according to previous research, particle size smaller than 40 nm contributes to the preparation of transparent dispersions and lifts the intensity of visible-light transmission rapidly.<sup>38</sup> Therefore, the smaller particle size obtained from RPB should be responsible for the better visual transparency and higher visible-light transmittance.

Figure 5 shows the TEM images and average particle sizes of MgAl-LDH nanoparticles prepared using an RPB (2400 rpm) without or with a hydrothermal treatment at different temperatures along with the corresponding digital photographs of dispersions (1 wt %) and their UV–vis curves on light transmittance. Clearly, the average particle size increases after hydrothermal treatment on gradually increasing the temperature from 90 to 130 °C. The results for those four samples are measured as 31, 65, 69, and 72 nm. However, the dispersibility of particles does not deteriorate with the increase of particle size. In addition, the morphology of particles changes from irregular shapes into hexagonal nanoflakes, and this trend becomes more and more obvious with the rise of temperature. This phenomenon could be explained by Ostwald ripening, which includes a dissolution–reprecipitation process. From the light transmittance curves, we can see that the value at 555 nm decreases from 77.4 to 63.9%, 62.3 and 61.2% after hydrothermal treatment at 90, 110, and 130 °C, respectively. Although the light loss is inevitable, nearly 80% of the original visible-light transmittance at 555 nm is still maintained even after hydrothermal treatment at 130 °C. Correspondingly, the optical transparency of dispersions declines only slightly after hydrothermal treatment. This operation gives the products a much wider range of potential applications, such as in the fields of nanocomposites, transparent films, and self-assembled materials.

Figure 6 presents the XRD patterns of MgAl-LDH nanoparticles prepared using an RPB (2400 rpm) without or with a hydrothermal treatment at different temperatures and an illustration of the possible formation process of these particles. From Figure 6a, the MgAl-LDH nanoparticles change from low crystallized to highly crystallized after hydrothermal treatment at 110 °C or even at a higher temperature, since increasing temperature is usually conducive to the recrystallization process of nanoparticles from low crystallinity to high crystallinity. According to the crystal structure of these particles, the metal cations ( $\text{Mg}^{2+}$  and  $\text{Al}^{3+}$ ) occupy the centers of edge-sharing octahedrons, whose vertexes contain hydroxide anions, making the octahedrons electrically neutral, and connect to form two-dimensional (2D) layers.<sup>3</sup> In addition, the growth rates of the (110) and (003) crystal planes are determined by the formation rate of bonds among  $\text{Mg}^{2+}$ ,  $\text{Al}^{3+}$ , and  $\text{OH}^-$  and the stacking rate between layers, respectively. Therefore, hydrothermal treatment under a high temperature boosts the dissolution–reprecipitation process (Ostwald ripening), which means an acceleration of the growth of particles, as well as the (110) and (003) crystal planes. As a result, MgAl-LDH nanoplates with hexagonal shapes and a layered structure can be successfully prepared, as shown in Figure 6b. The values of the  $\zeta$ -potential are 55.4, 48.6, 45.2, and 43.5 mV for those four samples according to the test

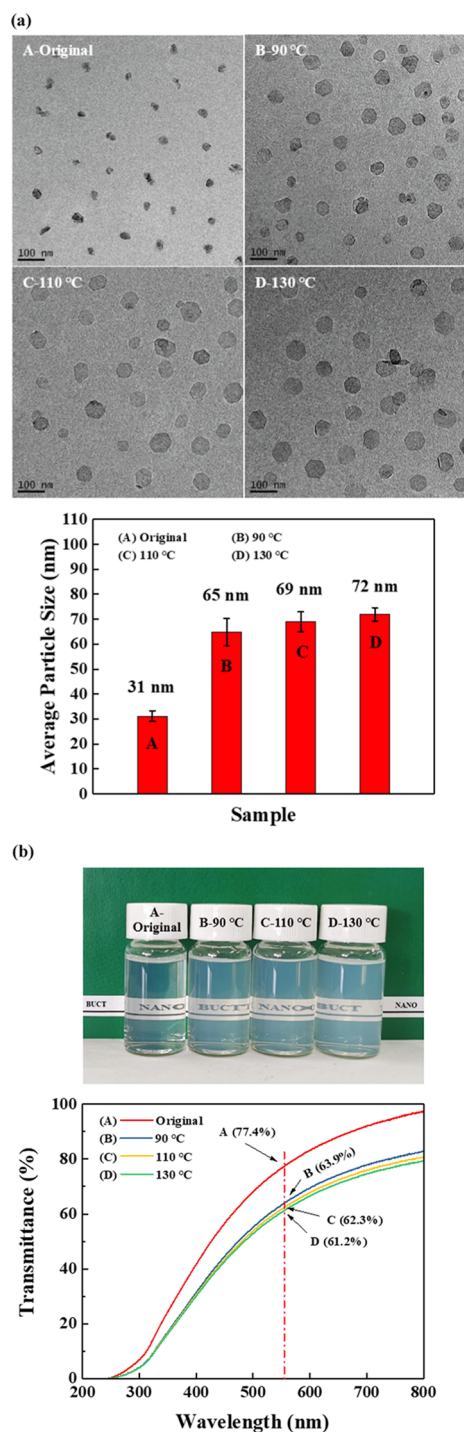


**Figure 5.** (a) TEM images and the average particle sizes of MgAl-LDH nanoparticles prepared by an RPB (2400 rpm) without or with a hydrothermal treatment at different temperatures and (b) corresponding digital photographs of dispersions (1 wt %) and their UV–vis curves on light transmittance.

results. This means that the excellent dispersibility of MgAl-LDH nanoparticles mainly depends on the high  $\zeta$ -potential.

Figure 7 displays the TG analysis results of MgAl-LDH nanoparticles prepared using an RPB (2400 rpm) without or with a hydrothermal treatment at 130 °C. Both samples were predried in a vacuum desiccator at 30 °C for 24 h before the TG analysis. From the weight-loss curves, it can be clearly seen that both samples experience a similar three-step weight loss

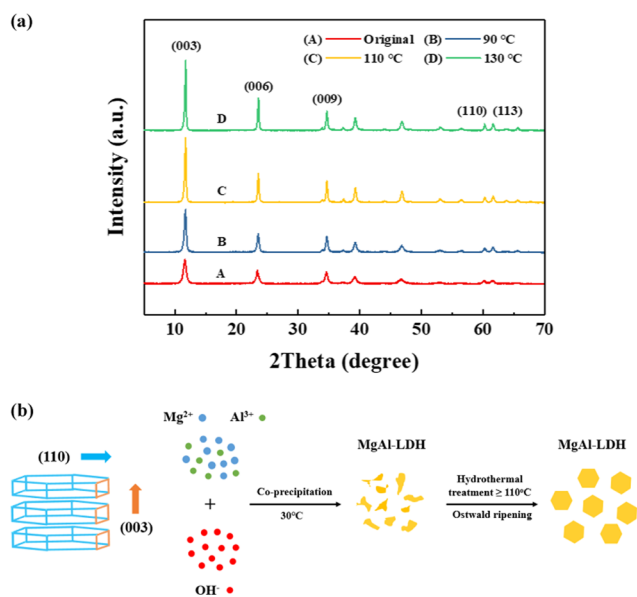


**Figure 6.** (a) XRD patterns of MgAl-LDH nanoparticles prepared using an RPB (2400 rpm) without or with a hydrothermal treatment at different temperatures and (b) illustration of the possible formation process of these particles.

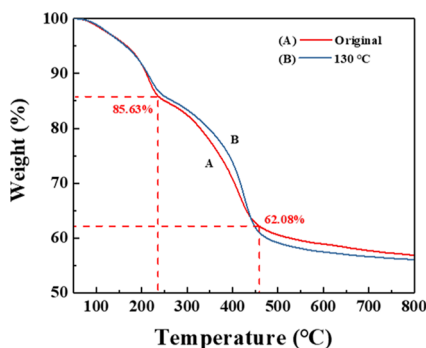


**Figure 7.** TG analysis results of MgAl-LDH nanoparticles prepared using an RPB (2400 rpm) without or with a hydrothermal treatment at 130 °C.

process. The first stage for the untreated sample is observed in the range of 50–235 °C, corresponding to a value of 14.37 wt %. This part is mainly caused by the removal of interlayer water and a small amount of surface-adsorbed water. The second stage starts from 235 to 460 °C, giving a result of 23.58 wt %, mainly ascribed to the decomposition of metal hydroxides and a part of carbonate anions. The last step is due to the decomposition of the rest of the carbonate anions, resulting in the release of CO<sub>2</sub>. Compared with the untreated sample, the hydrothermally treated sample achieves a little higher value in total weight loss, but the reason needs further investigation. According to the general formula of MgAl-LDHs and the value of Mg/Al employed in our study, we can calculate a specific formula of [Mg<sub>3</sub>Al(OH)<sub>2</sub>](CO<sub>3</sub>)<sub>0.5</sub>·nH<sub>2</sub>O ( $n = 2.2\text{--}2.3$ ) for the as-prepared products. Due to the release of a large amount of H<sub>2</sub>O and CO<sub>2</sub> in the decomposition process, the as-prepared MgAl-LDH nanoparticles have a promising prospect to be used as efficient and environmentally friendly fire-retardant additives.

Figure 8 exhibits two kinds of nanocomposite films, which consist of PVA and the MgAl-LDH nanoparticles prepared



**Figure 8.** Transparent nanocomposite films consisting of PVA and MgAl-LDH nanoparticles prepared using an RPB (2400 rpm) with a hydrothermal treatment at 130 °C.

using an RPB (2400 rpm) with a hydrothermal treatment at 130 °C. The contents of MgAl-LDH nanoparticles in these films are set to 10 wt %. Obviously, the (PVA/LDH)<sub>n</sub> ( $n = 1\text{--}10$ ) films are fabricated with high optical transparency. This indicates that the PVA and MgAl-LDH nanoparticles still maintain a well-dispersed state after evaporation of the solvent. Compared with the (PVA/LDH)<sub>n</sub> films, the (PVA+LDH)<sub>n</sub> films have almost the same excellent transparency, demonstrating a good compatibility and dispersibility between the PVA and MgAl-LDH nanoparticles. In addition, all nanocomposite films have outstanding flexibility. However, they are very sticky when they are peeled off from the substrate, which is decided by the nature of PVA. In fact, PVA has been widely used for paper coating, so the as-prepared nanocomposite films have a very high potential of being used for making refractory paper. In addition, due to the excellent particle dispersibility, optical transparency, and outstanding compatibility with certain polymer materials, these transparent MgAl-LDH dispersions may have rather extensive potential applications, such as in the fields of optical devices, catalysts, biomaterials, and self-assembled materials.

#### 4. CONCLUSIONS

In this study, stable transparent dispersions of monodispersed CO<sub>3</sub><sup>2-</sup>-intercalated MgAl-LDH nanoparticles were successfully prepared without any surface modification using a high-gravity-assisted coprecipitation approach in an RPB reactor, followed by a hydrothermal process. The monodispersed nanoparticles prior to hydrothermal treatment have an average particle size of 31 nm, and the visible-light transmittance of nano-dispersions can reach up to 77.4% at 555 nm. The RPB-prepared products have smaller particle sizes, narrower size distributions, and better visual transparency than those prepared by STR. The reaction time is greatly shortened from 20 min to 20 s, realizing a continuous synthesis. Further

hydrothermal treatment can create regular hexagonal-shaped LDH nanoparticles with increased sizes. The optical transparency of nanodispersions can be well maintained. High  $\zeta$ -potential is considered as the main reason for the excellent stability of dispersed MgAl-LDH nanoparticles. In addition, transparent PVA-based nanocomposite films containing MgAl-LDH nanoparticles were also fabricated by using the spin-coating method and the layer-by-layer technique, demonstrating an excellent compatibility and dispersibility between PVA and MgAl-LDH nanoparticles after evaporation of the solvent. In summary, this approach provides an idea to prepare surfactant-free transparent dispersions of monodispersed MgAl-LDH nanoparticles, which may have a wide range of potential applications in many fields, such as nanocomposites, catalysts, transparent films, and self-assembled materials.

## AUTHOR INFORMATION

### Corresponding Author

**Jie-Xin Wang** – Beijing Advanced Innovation Center for Soft Matter Science and Engineering, State Key Laboratory of Organic-Inorganic Composites and Research Center of the Ministry of Education for High Gravity Engineering and Technology, Beijing University of Chemical Technology, Beijing 100029, P. R. China; [orcid.org/0000-0003-0459-1621](https://orcid.org/0000-0003-0459-1621); Email: [wangjx@mail.buct.edu.cn](mailto:wangjx@mail.buct.edu.cn)

### Authors

**Bo Chen** – Beijing Advanced Innovation Center for Soft Matter Science and Engineering, State Key Laboratory of Organic-Inorganic Composites and Research Center of the Ministry of Education for High Gravity Engineering and Technology, Beijing University of Chemical Technology, Beijing 100029, P. R. China

**Qian Sun** – Beijing Advanced Innovation Center for Soft Matter Science and Engineering, State Key Laboratory of Organic-Inorganic Composites, Beijing University of Chemical Technology, Beijing 100029, P. R. China

**Dan Wang** – Beijing Advanced Innovation Center for Soft Matter Science and Engineering, State Key Laboratory of Organic-Inorganic Composites, Beijing University of Chemical Technology, Beijing 100029, P. R. China; [orcid.org/0000-0002-3515-4590](https://orcid.org/0000-0002-3515-4590)

**Xiao-Fei Zeng** – Research Center of the Ministry of Education for High Gravity Engineering and Technology, Beijing University of Chemical Technology, Beijing 100029, P. R. China; [orcid.org/0000-0001-9010-0088](https://orcid.org/0000-0001-9010-0088)

**Jian-Feng Chen** – Beijing Advanced Innovation Center for Soft Matter Science and Engineering, State Key Laboratory of Organic-Inorganic Composites and Research Center of the Ministry of Education for High Gravity Engineering and Technology, Beijing University of Chemical Technology, Beijing 100029, P. R. China; [orcid.org/0000-0003-1947-0603](https://orcid.org/0000-0003-1947-0603)

Complete contact information is available at:  
<https://pubs.acs.org/10.1021/acs.iecr.9b06272>

### Notes

The authors declare no competing financial interest.

## ACKNOWLEDGMENTS

This work was financially supported by the National Key Research and Development Program of China (2016YFA0201701/2016YFA0201700) and the National Natural Science Foundation of China (21576022, 21622601,

and 21878015). B.C. is very grateful to Prof. Stuart Clarke for his guidance when B.C. studied at the University of Cambridge.

## REFERENCES

- (1) Mishra, G.; Dash, B.; Pandey, S. Layered double hydroxides: A brief review from fundamentals to application as evolving biomaterials. *Appl. Clay Sci.* **2018**, *153*, 172–186.
- (2) Daud, M.; Kamal, M. S.; Shehzad, F.; Al-Harathi, M. A. Graphene/Layered double hydroxides nanocomposites: A review of recent progress in synthesis and applications. *Carbon* **2016**, *104*, 241–252.
- (3) Wang, Q.; O'Hare, D. Recent advances in the synthesis and application of layered double hydroxide (LDH) nanosheets. *Chem. Rev.* **2012**, *112*, 4124–4155.
- (4) Yu, J. F.; Wang, Q.; O'Hare, D.; Sun, L. Y. Preparation of two dimensional layered double hydroxide nanosheets and their applications. *Chem. Soc. Rev.* **2017**, *46*, 5950–5974.
- (5) Gu, Z.; Atherton, J. J.; Xu, Z. P. Hierarchical layered double hydroxide nanocomposites: Structure, synthesis and applications. *Chem. Commun.* **2015**, *51*, 3024–3036.
- (6) Taviot-Gu  ho, C.; Pr  vot, V.; Forano, C.; Renaudin, G.; Mousty, C.; Leroux, F. Tailoring hybrid layered double hydroxides for the development of innovative applications. *Adv. Funct. Mater.* **2018**, *28*, No. 1703868.
- (7) Zhao, M. Q.; Zhang, Q.; Huang, J. Q.; Wei, F. Hierarchical nanocomposites derived from nanocarbons and layered double hydroxides - Properties, synthesis, and applications. *Adv. Funct. Mater.* **2012**, *22*, 675–694.
- (8) Theiss, F. L.; Ayoko, G. A.; Frost, R. L. Synthesis of layered double hydroxides containing  $Mg^{2+}$ ,  $Zn^{2+}$ ,  $Ca^{2+}$  and  $Al^{3+}$  layer cations by co-precipitation methods - A review. *Appl. Surf. Sci.* **2016**, *383*, 200–213.
- (9) Sun, W.; Wu, T. T.; Wang, L. D.; Dong, C.; Liu, G. C. Controlled preparation of MgAl-Layered double hydroxide/graphene hybrids and their applications for metal protection. *Ind. Eng. Chem. Res.* **2019**, *58*, 16516–16525.
- (10) Iyi, N.; Ebina, Y.; Sasaki, T. Water-swellable MgAl-LDH (Layered double hydroxide) hybrids: Synthesis, characterization, and film preparation. *Langmuir* **2008**, *24*, 5591–5598.
- (11) Jamil, S.; Alvi, A. R.; Khan, S. R. Layered double hydroxides (LDHs): Synthesis & Applications. *Prog. Chem.* **2019**, *31*, 394–412.
- (12) Liang, D.; Yue, W.; Sun, G.; Zheng, D.; Ooi, K.; Yang, X. Direct synthesis of unilamellar MgAl-LDH nanosheets and stacking in aqueous solution. *Langmuir* **2015**, *31*, 12464–12471.
- (13) Hassanzadeh-Aghdam, M. K.; Ansari, R.; Mahmoodi, M. J.; Darvizeh, A. Effect of nanoparticle aggregation on the creep behavior of polymer nanocomposites. *Compos. Sci. Technol.* **2018**, *162*, 93–100.
- (14) Slade, W. H.; Boss, E.; Russo, C. Effects of particle aggregation and disaggregation on their inherent optical properties. *Opt. Express* **2011**, *19*, 7945–7959.
- (15) Wang, X.; Li, Y. D. Monodisperse nanocrystals: general synthesis, assembly, and their applications. *Chem. Commun.* **2007**, 2901–2910.
- (16) Gong, M. G.; Ewing, D.; Casper, M.; Stramel, A.; Elliot, A.; Wu, J. Z. Controllable synthesis of monodispersed  $Fe_{1-x}S_2$  nanocrystals for high performance optoelectronic devices. *ACS Appl. Mater. Interfaces* **2019**, *11*, 19286–19293.
- (17) Li, J. Z.; Wang, H. F.; Lin, L.; Fang, Q.; Peng, X. Quantitative identification of basic growth channels for formation of monodisperse nanocrystals. *J. Am. Chem. Soc.* **2018**, *140*, 5474–5484.
- (18) Zhao, Y.; Li, F.; Zhang, R.; Evans, D. G.; Duan, X. Preparation of layered double-hydroxide nanomaterials with a uniform crystallite size using a new method involving separate nucleation and aging steps. *Chem. Mater.* **2002**, *14*, 4286–4291.
- (19) Pang, X. J.; Sun, M. Y.; Ma, X. M.; Hou, W. G. Synthesis of layered double hydroxide nanosheets by coprecipitation using a T-type microchannel reactor. *J. Solid State Chem.* **2014**, *210*, 111–115.

- (20) Daud, M.; Hai, A.; Banat, F.; Wazir, M. B.; Habib, M.; Bharath, G.; Al-Harathi, M. A. A review on the recent advances, challenges and future aspect of layered double hydroxides (LDH)-Containing hybrids as promising absorbents for dyes removal. *J. Mol. Liq.* **2019**, *288*, No. 110989.
- (21) Layrac, G.; Destarac, M.; Gérardin, C.; Tichit, D. Highly stable layered double hydroxide colloids: A direct aqueous synthesis route from hybrid polyion complex micelles. *Langmuir* **2014**, *30*, 9663–9671.
- (22) Yu, J. F.; Liu, J. J.; Clearfield, A.; Sims, J. E.; Speigle, M. T.; Suib, S. L.; Sun, L. Y. Synthesis of layered double hydroxide single-layer nanosheets in formamide. *Inorg. Chem.* **2016**, *55*, 12036–12041.
- (23) de Beer, M. M.; Andre, K.; Henk, V.; Gerrald, B.; Riaan, S. Intensified and flexible flash degassing in a rotating packed bed. *Ind. Eng. Chem. Res.* **2018**, *57*, 14261–14272.
- (24) Chen, Q. Y.; Chu, G. W.; Luo, Y.; Sang, L.; Zhang, L. L.; Zou, H. K.; Chen, J. F. Polytetrafluoroethylene wire mesh packing in a rotating packed bed: Mass-Transfer studies. *Ind. Eng. Chem. Res.* **2016**, *55*, 11606–11613.
- (25) Bao, J.; Wang, J. X.; Zeng, X. F.; Zhang, L. L.; Chen, J. F. Large-scale synthesis of uniform silver nanowires by high-gravity technology for flexible transparent conductive electrode. *Ind. Eng. Chem. Res.* **2019**, *58*, 20630–20638.
- (26) Lin, C. C.; Lin, Y. C. Preparation of ZnO nanoparticles using a rotating packed bed. *Ceram. Int.* **2016**, *42*, 17295–17302.
- (27) Kang, F.; Wang, D.; Pu, Y.; Zeng, X. F.; Wang, J. X.; Chen, J. F. Efficient preparation of monodisperse  $\text{CaCO}_3$  nanoparticles as overbased nanodetergents in a high-gravity rotating packed bed reactor. *Powder Technol.* **2018**, *325*, 405–411.
- (28) Sun, Q.; Chen, B.; Wu, X.; Wang, M.; Zhang, C.; Zeng, X. F.; Wang, J. X.; Chen, J. F. Preparation of transparent suspension of lamellar magnesium hydroxide nanocrystals using a high-gravity reactive precipitation combined with surface modification. *Ind. Eng. Chem. Res.* **2015**, *54*, 666–671.
- (29) Zhang, N.; Ren, X. J.; Guo, Y. J.; Liu, Z. W.; Liu, Y. Z. Impinging stream-Rotating packed bed reactor combination coprecipitation synthesis of cobalt-manganese-layered double hydroxide for electrode materials. *Energy Technol.* **2019**, *7*, No. 1900156.
- (30) Xu, S.; Liao, M. C.; Zeng, H. Y.; Zhang, Z. Q.; Liu, X. J.; Zhu, P. H. Ultrafine hydrotalcite particles prepared with novel technology to improve the flame retardancy of polypropylene. *Appl. Clay Sci.* **2015**, *108*, 215–221.
- (31) Tichit, D.; Layrac, G.; Gérardin, C. Synthesis of layered double hydroxides through continuous flow processes: A review. *Chem. Eng. J.* **2019**, *369*, 302–332.
- (32) Abelló, S.; Mitchell, S.; Santiago, M.; Stoica, G.; Pérez-Ramirez, J. Perturbing the properties of layered double hydroxides by continuous coprecipitation with short residence time. *J. Mater. Chem.* **2010**, *20*, 5878–5887.
- (33) Abelló, S.; Pérez-Ramirez, J. Tuning nanomaterials' characteristics by a miniaturized in-line dispersion-precipitation method: Application to hydrotalcite synthesis. *Adv. Mater.* **2006**, *18*, 2436–2439.
- (34) Chen, J. F.; Shao, L. Mass production of nanoparticles by high gravity reactive precipitation technology with low cost. *China Particul.* **2003**, *1*, 64–69.
- (35) Chen, J. F.; Wang, Y. H.; Guo, F.; Wang, X. M.; Zheng, C. Synthesis of nanoparticles with novel technology: High-gravity reactive precipitation. *Ind. Eng. Chem. Res.* **2000**, *39*, 948–954.
- (36) Yue, X. J.; Luo, Y.; Chen, Q. Y.; Chu, G. W.; Luo, J. Z.; Zhang, L. L.; Chen, J. F. Investigation of micromixing and precipitation process in a rotating packed bed reactor with PTFE packing. *Chem. Eng. Process.* **2018**, *125*, 227–233.
- (37) Wang, Z.; Yang, T.; Liu, Z.; Wang, S.; Gao, Y.; Wu, M. Mass transfer in a rotating packed bed: A critical review. *Chem. Eng. Process.* **2019**, *139*, 78–94.
- (38) Althues, H.; Henle, J.; Kaskel, S. Functional inorganic nanofillers for transparent polymers. *Chem. Soc. Rev.* **2007**, *36*, 1454–1465.